RSC Advances

PAPER

View Article Online
View Journal | View Issue

Cite this: *RSC Adv.*, 2026, **16**, 28931

Iridium–Schiff base complex-based fluorimetric turn-off sensor and HPLC-DAD analytical approaches for quantitation of 8-hydroxy-2′-deoxyguanosine as an oxidative DNA damage biomarker in biofluids of healthy and diabetic subjects

Hazim M. Ali, *[a] Tamer H. A. Hasanin,[a] Ahmed Hamad Alanazi,[a] Emad Manni,[b] Moamen S. Refat,[c] Azza H. Rageh[d] and Mohammed Gamal *[e]

8-Hydroxy-2′-deoxyguanosine (8-OHdG) is a well-established biomarker of oxidative DNA damage formed through reactive oxygen species-mediated oxidation of guanosine residues. It is widely recognized as a laboratory biomarker of oxidative DNA damage and has been associated with carcinogenic progression. In this study, a novel, rapid, and highly selective spectrofluorometric platform was developed based on quenching of the fluorescence of a newly synthesized iridium–Schiff base complex by 8-OHdG; an HPLC-DAD method was also developed for confirmatory quantification. The iridium–Schiff complex exhibited intrinsic green fluorescence at λ_{em} = 500 nm upon excitation at λ_{ex} = 292 nm. The optimal fluorescence intensity and pronounced quenching effect of 8-OHdG were achieved in an acetate buffer solution with pH 3.6. Both methods exhibited wide linearity ranges: 0.025–20 μg mL^{-1} for spectrofluorimetry and 0.005–50 μg mL^{-1} for HPLC-DAD. The limits of detection (LODs) were 0.0179 μg mL^{-1} and 0.0013 μg mL^{-1}, respectively. High accuracy and precision were confirmed with recovery percentages ranging from 97.142% to 100.006% for the spectrofluorimetric method and 95.321% to 99.399% for HPLC-DAD. Moreover, relative standard deviation values (RSD%) ranges did not exceed 0.266–2.05% and 0.604–1.984%, respectively confirming the high reproducibility of the developed approaches. For minimizing matrix interference from endogenous substances such as creatinine and uric acid, samples were pretreated using Strata C18-E solid-phase extraction cartridges prior to analysis. The novel methods coupled with Strata C18-E (SPE) were successfully validated and applied to the analysis of 8-OHdG in 40 human urine and serum samples obtained from healthy and diabetic patient volunteers. Detectable levels of 8-OHdG were found in 36 out of 40 samples, ranging from 0.013 to 15.766 μg mL^{-1}. Furthermore, both analytical approaches for the detection of 8-OHdG are in alignment with the principles of white and green analytical chemistry, offering environmentally friendly, efficient, and straightforward analytical procedures. Accordingly, the proposed methods exhibit considerable promise for the determination of urinary 8-OHdG, which serves as a reliable biomarker of oxidative stress in a range of pathological conditions owing to its diagnostic relevance as an oxidative DNA damage biomarker.

Received 13th March 2026
Accepted 15th May 2026

DOI: 10.1039/d6ra02144a

rsc.li/rsc-advances

1 Introduction

Reactive oxygen species (ROS) are highly reactive oxygen-derived molecules, such as superoxide anion radical, hydrogen peroxide, singlet oxygen, and hydroxyl radical.[1] ROS are continuously generated in living systems, primarily as by-products of mitochondrial oxidative metabolism. Although ROS play important roles in normal cellular signaling, their excessive production can lead to oxidative damage of essential biomolecules within the cells, including proteins, membrane

[a]*Department of Chemistry, College of Science, Jouf University, P.O. Box 2014, Sakaka, Aljouf, Saudi Arabia. E-mail: hmali@ju.edu.sa*

[b]*Department of Clinical Laboratory Sciences, College of Applied Medical Sciences, Jouf University, Saudi Arabia*

[c]*Department of Chemistry, College of Science, Taif University, P.O. Box 11099, Taif, 21944, Saudi Arabia*

[d]*Department of Pharmacognosy and Pharmaceutical Chemistry, College of Pharmacy, Taibah University, Al-Madinah Al-Munawarah 30001, Saudi Arabia*

[e]*Department of Pharmaceutical Analytical Chemistry, Faculty of Pharmacy, Beni-Suef University, Alshaheed Shehata Ahmed Hegazy St., Beni-Suef 62574, Egypt. E-mail: mgamalm3000@yahoo.com*

phospholipids, and DNA, leading to cellular dysfunction, apoptosis, and death.[2–5]

Oxidative attack on DNA induces chemical modifications of 2′-deoxyribonucleosides, generating several oxidized derivatives, such as 8-hydroxy-2′-deoxyguanosine (8-OHdG), which is the predominant and most investigated product. It is widely known as a sensitive and reliable method for assessing oxidative DNA damage in biological systems.[6] Evidence also indicates that oxidative DNA injury represents a pivotal function in the pathogenesis of numerous diseases, particularly neurodegenerative and malignant disorders[7,8]

In addition, 8-OHdG exhibits mutagenic properties and may exert other damaging properties on cellular functions, including enhanced microsatellite instability and speeding up of telomere attrition[9]

Given the diagnostic relevance of alterations in 8-OHdG levels, there is a clear need for reliable non-invasive analytical methodologies capable of evaluating oxidative DNA damage, correlating these changes with exposure to ROS-generating factors.[10]

Therefore, the accurate quantification of 8-OHdG in complex biological matrices is challenging due to its trace-level concentrations and the presence of endogenous substances that may interfere in biosamples.[10–13] Consequently, the development of selective and sensitive strategies for the determination of urinary 8-OHdG remains a significant analytical challenge.

Several analytical approaches were employed for measuring 8-OHdG in different matrices, including capillary electrophoresis[14,15] HPLC coupled with electrochemical detection (HPLC-ECD),[16] HPLC with ultraviolet detection (HPLC-UV),[17,18] liquid chromatography-mass spectrometry (LC-MS),[19] electrochemical analysis,[20–23] colorimetric assays[24,25] and fluorometric assays.[26,27] Previous spectrophotometric methods provide high sensitivity and broad working range detection. However, they often require prolonged incubation times to ensure stabile interaction between fluorescent probe and 8-OHdG prior to analysis.[24–27]

Due to these limitations, a highly sensitive, selective, time-efficient, cost-effective, and user-friendly analytical strategy for the detection of 8-OHdG was developed based on the intrinsic fluorescence quenching of the iridium–Schiff base complex. In addition, an HPLC-DAD method was established to confirm the spectrofluorometric findings for the estimation of 8-OHdG. The two methods were applied to the assay of 8-OHdG in urine and serum samples collected from healthy and diabetic volunteer patients. Finally, comprehensive whiteness and green assessment tools were tailored to estimate the environmental impact, profile saving, and sustainability of the developed analytical procedures.

2 Experimental

2.1 Materials and reagents

2-Amino-9-[(2*R*,4*S*,5*R*)-4-hydroxy-5-(hydroxyl methyl) oxolan-2-yl]-3,7-dihydropurine-6,8-dione (8-hydroxy-2′-deoxyguanosine, 8-OHdG) illustrated in (SI Scheme 1A) with an indicated purity of 95% was supplied by Biosynth Ltd (Compton, United Kingdom). *p*-Aminoacetophenone and 2,4-dihydroxybenzaldehyde were obtained from CNW Technologies GmbH (Düsseldorf, Germany). Analytical grade reagents, including pentoxifylline (used as the HPLC internal standard; SI Scheme 1B). $IrCl_3 \cdot xH_2O$, methanol, 2-propanol, ethanol, acetonitrile, acetone, acetic acid (CH_3COOH), phosphoric acid (H_3PO_4), hydrochloric acid (HCl), sodium hydroxide (NaOH), sodium acetate, monosodium dihydrogen phosphate, disodium monohydrogen phosphate, ammonium hydroxide and trichloroacetic acid were purchased from Sigma-Aldrich (St. Louis, USA). All aqueous preparations were carried out using deionized water.

2.2 Description of analytical methods

2.2.1 Synthesis of the fluorescent sensor Ir-SB complex. The Schiff base ligand (*E*)-1-[4-(2,4-dihydroxybenzylidene) amino] ethenone (SB, Scheme 1) was synthesized following a previously described protocol with slight adaptation.[28] The synthesis procedure was conducted as follows: 2,4-dihydroxybenzaldehyde (DHB, 50 mmol) was dissolved in 50 mL of hot methanol, and *p*-aminoacetophenone (AA, 25 mmol) was

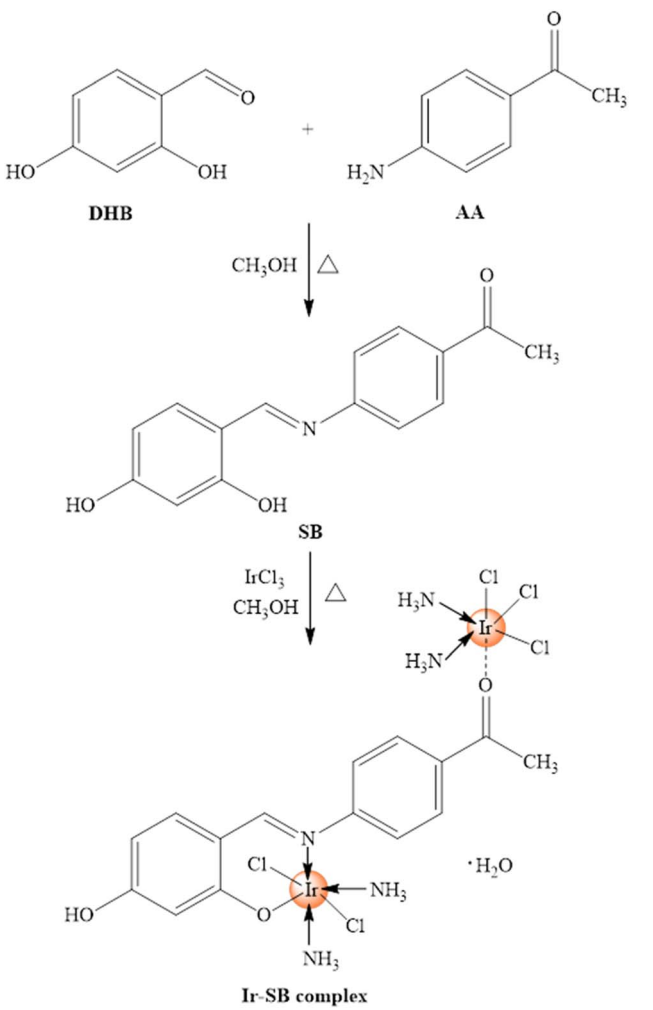

Scheme 1 Molecular structure of Ir-SB complex.

added to the stirred solution. The mixture was refluxed for three hours with continuous stirring. Upon completion, it was cooled to room temperature, filtered to yield a yellow solid, washed successively with hot methanol and diethyl ether, and dried under vacuum at 110 °C in the presence of anhydrous $CaCl_2$. The purified Schiff base has been obtained as a pale-yellow solid approximately 80% yield. The photoluminescent iridium complex-(*E*)-1-[4-(2,4-dihydroxybenzylidene)amino] ethenone (Ir-SB complex) was synthesized according to the previously established method.[28] In a typical procedure, a precise quantity of the SB ligand (10 mmol) was dissolved in 50 mL of hot methanol and mixed with $IrCl_3 \cdot xH_2O$ (5 mmol). A few drops of concentrated ammonium hydroxide were then added dropwise with continuous stirring until the pH of the reaction mixture reached 8–9 to promote complex formation. The reaction mixture was refluxed at 70 °C for 2 h with stirring, after which the solvent was evaporated to reduce the volume by half. The resulting solid complex was isolated by filtration, thoroughly washed with methanol and diethyl ether, and dried under vacuum over calcium chloride ($CaCl_2$). The complex of Ir-SB was obtained as a reddish-brown solid in approximately 80% yield.

2.2.2 Preparation of the Ir-SB complex sensor and 8-OHdG analyte. For the preparation of the Ir-SB complex solution, 10 mg of the Ir-SB complex was dispersed in 50 mL of distilled water, ultrasonicated for 30 min and left to stand overnight to reach equilibrium. The mixture was filtered through a 0.20 μm syringe filter (Advantec Toyo, Japan), and the filtrate was used for further experiments. On the other hand, a stock standard solution of 8-hydroxy-2′-deoxyguanosine was prepared by dissolving 10 mg of 8-OHdG in 50 mL methanol, yielding a final concentration of 200 μg mL^{-1}.

2.2.3 Preparations and measurements of working solutions. Aliquots containing various concentrations of 8-OHdG were transferred into a dry, clean 5 mL volumetric flask, followed by the addition of 0.2 mL of 5 μg mL^{-1} of Ir-SB complex solution. The mixture was diluted to 5 mL with acetate buffer (pH 3.6) and vortexed thoroughly for 30 s. The same procedure was used for study the effect of phosphoric acid, hydrochloric acid, acetic acid, sodium hydroxide and phosphate buffer on the fluorescence intensity of Ir-SB complex. The fluorescence intensity of the Ir-SB complex from this solution was monitored, and an emission signal was recorded at $\lambda_{em} = 500$ nm (slits, 20 nm) after applying excitation at $\lambda_{ex} = 292$ nm (slits, 5 nm). The influence of the various concentrations of 8-OHdG within the range of 0.025–60 μg mL^{-1} on the intensity of the emission signal of the Ir-SB complex probe was recorded, where a calibration curve was developed.

2.2.4 Sample collection and preparation. All experiments were performed in accordance with the Guidelines of the Declaration of Helsinki – the international standard for medical research involving human subjects, and experiments were approved by the ethics committee at Beni-Suef University. Written informed consent was obtained from human participants of this study. Urine and blood were collected as a spot sample from healthy and diabetic patient volunteers after approval by the Ethics Committee of Beni-Suef University, Faculty of Pharmacy, Beni-Suef Governorate, Egypt (Approval No. FPH-BSU-HREC-0001425). Forty samples were used in the present study and divided into ten urine samples and ten blood samples from healthy volunteers as well as ten urine samples and ten blood samples from diabetic patient volunteers. Blood samples were centrifuged to separate serum. Serum and urine samples were stored at −20 °C until analysis. The frozen urine and serum samples were thawed to room temperature prior to use. In experiments, 2.5 mL of urine and 0.5 mL of serum were used and treated with 0.5 mL of 0.1 M trichloroacetic acid (TCA) to precipitate proteins. The volume of the mixture was adjusted to 5 mL with deionized water and vortex-mixed for 30 seconds. The samples were centrifuged to remove the proteins, and the supernatant was loaded on solid-phase extraction cartridge (Strata C18-E (500 mg), Phenomenex, Torrance, USA), which had been initially conditioned with water (5 mL), followed by 5 mL of the appropriate organic solvent. SPE cartridges were rinsed with 15 mL of deionized water to remove matrix interference, and the sample was subsequently eluted using 5 mL of methanol. To determine the amount of 8-OHdG, the resulting solution fraction was directly injected into the HPLC-DAD system, and 200 μL of the remaining eluate was used for spectrofluorimetric analysis according to the procedure described in section 2.2.3. In contrast, method accuracy and assessment of 8-OHdG were evaluated by spiking urine and serum samples with known concentrations of 8-OHdG, and the previous procedure was followed.

2.3 Instrumentation

UV-visible absorption measurements were conducted using a Cary-60UV-Vis spectrophotometer (Agilent Technologies). Fluorescence measurements were performed using a Cary Eclipse fluorescence spectrophotometer (Agilent Technologies, USA), using a 1.0 cm quartz cuvette. The excitation and emission slit width were adjusted to 5 nm and 20 nm, respectively. The chromatographic analysis (HPLC method) was performed on a Thermo Scientific Dionex UltiMate 3000 UHPLC+ system equipped with a DAD-3000 diode array detector. Data recording was performed using the Chromeleon™ 7.2 Chromatography Data System.

2.4 Chromatographic conditions (HPLC method)

The quantitative separation of 8-OHdG using pentoxifylline as an internal chromatographic standard was accomplished using a Thermo Acclaim™ 120C18 (150 × 4.6 mm, 5 μm particle size) (Thermo Fisher Scientific, USA). The mobile liquid system consisted of 0.1% aqueous formic acid and methanol in a volumetric ratio of 10 : 90 (v/v) delivered under isocratic settings at a flow rate of 0.5 mL min^{-1}, with detection and quantitation of 8-OHdG at a wavelength of 250 nm. The volume of the injection for both standards and biological samples was 10 μL.

2.5 Validation of the new analytical approaches

The developed spectrofluorometric and HPLC-DAD approaches for 8-OHdG quantification were validated according to performance criteria, including accuracy, linearity, precision, limits of

detection (LOD), and quantification (LOQ). Linearity of the two novel approaches was evaluated using thirteen calibration levels across-concentration ranges of 0.025 to 60 μg mL^{-1} (spectrofluorometric method) and 0.005 to 60 μg mL^{-1} and (HPLC-DAD method). Accuracy and precision were estimated at three levels of 8-OHdG (0.06, 5, and 15 μg mL^{-1}). Accuracy values were expressed as recovery percentages, calculated as: recovery (%) = (measured value/added value) × 100. Precisions was expressed as relative standard deviation (RSD), calculated as: RSD (%) = (standard deviation (SD)/mean measured value) × 100. LOD and LOQ values were calculated based on the standard deviation of the calibration intercept (SD) and the slope (a) of the calibration curve using the well-known equations: LOD = 3 × SD/a and LOQ = 10 × SD/a, respectively.

3 Results and discussion

3.1 Fluorescence response mechanism

Photophysical interaction between the synthesized Ir-SB complex and 8-OHdG molecules was studied in terms of excitation and emission spectral analyses. As depicted in Fig. 1, the Ir-SB complex exhibits a single intense emission band centered at ~500 nm (spectrum A) when excited at 292 nm. The band shape is nearly symmetric and featureless, consistent with an allowed charge-transfer/ligand-centered transition typical of an iridium Schiff-base complex. Upon addition of 8-OHdG (spectrum B), the maximum emission wavelength remains essentially unchanged, whereas the intensity drops substantially, indicating a classic "turn-off" response dominated by quenching rather than by the formation of a new emissive species. The corresponding excitation spectra recorded at 500 nm (spectra C and D) further support this finding: both Ir-SB alone and the Ir-SB-8-OHdG system share the same excitation maximum at ~292 nm, but the overall excitation intensity is reduced in the presence of 8-OHdG. Interestingly, at λ_{ex} = 292 nm, 8-OHdG did not show a fluorescence signal; thus, it has no interference during monitoring the Ir-SB complex fluorescence signal.

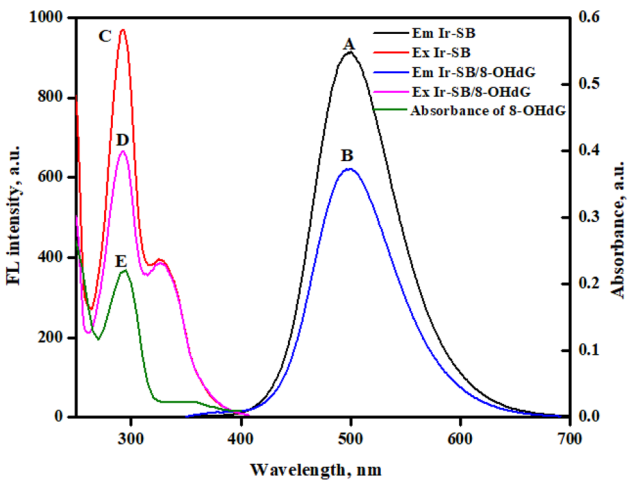

Fig. 1 Emission spectra of Ir-SB complex (line A) and Ir-SB complex-8-OHdG (line B) at λ_{ex} = 292 nm and excitation spectra of Ir-SB complex (line C) and Ir-SB complex-8-OHdG (line D) at λ_{em} = 500 nm. Absorption spectrum of 8-OHdG with λ_{max} = 292 nm (line E). The used concentrations; 0.2 μg mL^{-1} of Ir-SB complex and 5 μg mL^{-1} of 8-OHdG.

The aforementioned spectroscopic observations are visually illustrated in Fig. S1. As seen, under 254 nm UV illumination, the Ir-SB complex in the left-side cuvette shows a green luminescence, whereas cuvettes containing solutions of Ir-SB-8-OHdG gradually fade as the 8-OHdG concentration increases, demonstrating that the quenching is intense enough to be recognized by the naked eye. Such clear luminescent variation under a simple UV lamp provides a preliminary visual indication in solution-phase 8-OHdG probes, where the diminished fluorescence of the Ir-SB complex under 254 nm can be exploited as an initial identification of the presence of 8-OHdG.

3.2 Optimization of experimental parameters for the Ir-SB probe

3.2.1 Solvent effect and pH. The fluorescence intensity of the Ir-SB complex shows a clear solvent-dependent behavior (Fig. S2), with emission intensity (λ_{ex} = 292 nm) being the highest in acetonitrile and water, followed by ethanol, methanol, DMSO, and almost complete quenching in isopropanol and acetone. The very strong emission in acetonitrile, a polar but relatively weakly coordinating aprotic solvent, points to efficient population of the MLCT/ligand-centered excited state with minimal competitive solvation of the Ir site. On the other hand, the Ir-SB complex in water exhibits a moderate intensity due to the fact that the complex remains intact and that hydrogen bonding to the phenolic/imine sites rigidifies the ligand framework without severely perturbing the metal–ligand charge-transfer (MLCT) state. The solvent was selected based on its ability to enhance the interaction between the Ir-SB complex and 8-OHdG. In the present case, water is preferred over acetonitrile because water enhances the interaction between 8-OHdG and Ir-SB complex.

On the other hand, the fluorescence intensity of the Ir-SB complex is markedly influenced by the pH of the surrounding medium, which reflects protonation–deprotonation equilibria for the SB functional groups and their influence on metal coordination and electronic transitions. As shown in Fig. S3, in purely acidic solutions at pH 3.0, the fluorescence is somewhat attenuated, but as the medium is converted to acetate buffer and the pH increases to 3.6–4.0, the intensity reaches a broad maximum with the highest fluorescence intensity observed in acetate buffer at pH 3.6. Beyond this window, a progressive increase of pH value from acetate to phosphate buffers and then to mildly alkaline conditions led to a monotonic decrease in emission, with a substantial loss of brightness above pH 7 and the weakest signal observed at pH 8.5. This behavior is characteristic of Schiff-base metal complexes in which the protonation state of phenolic and imine donor sites controls both the rigidity of the coordination sphere and the propensity for non-radiative deactivation.[29] At mildly acidic pH, the ligand is partially protonated yet remains strongly bound to Ir, giving a rigid, conjugated framework that favors radiative decay; at higher pH, deprotonation of phenolic groups can trigger

photoinduced electron transfer or partial hydrolysis of the complex, opening additional non-radiative channels and diminishing fluorescence.[29,30] Comparable pH-dependent trends have been reported for coumarin, graphitic carbon nitride, and photosensitizer-type 8-OHdG probes, which often display optimal performance in a narrow mildly acidic window tailored to the target matrix.[31,32] Finally, the acetate buffer at pH 3.6 seems to provide the most favorable balance between protonation and Ir-SB coordination, leading to the strongest emission.

3.2.2 Excitation wavelength effect. Fig. S4 examines the maximum emission dependency on excitation wavelength for the Ir-SB complex. The fluorescence intensity of the complex was found to be strongly dependent on the excitation wavelength, indicating the presence of specific electronic transitions within the complex. The maximum fluorescence intensity at 292 nm indicates that this wavelength corresponds to the most effective excitation of the complex's electronic states. At wavelengths below 292 nm, the fluorescence intensity is lower, likely due to less efficient absorption or non-radiative relaxation pathways competing with fluorescence. Conversely, excitation at wavelengths above 292 nm also produces lower intensity, which can be attributed to insufficient photon energy to promote electrons to the excited state responsible for emission. This behavior is consistent with typical fluorescence phenomena, where the emission intensity is maximized when the excitation energy closely matches the electronic transition of the fluorophore. Therefore, $\lambda_{ex} = 292$ nm was chosen to be the optimal working excitation wavelength.

3.3 Systematic optimization of HPLC parameters for enhanced separation efficiency

Several practical experiments were conducted to investigate the effect of various chromatographic parameters on the performance of the HPLC method developed for quantification of 8-OHdG. Many different acids and solvents were tested in various volumes to prepare the liquid mobile system, including methanol combined with 0.1% acetic acid in water, methanol with 0.1% formic acid in water, acetonitrile with 0.1% acetic acid in water, acetonitrile with 0.1% formic acid in water, methanol–water mixtures, and methanol–acetonitrile systems. In addition, chromatographic variables such as flow rates, column temperature, detection wavelengths, and stationary phase types were optimized to obtain adequate separation efficiency, improved peak area symmetry, satisfactory peak height and area, acceptable resolution, and reduced overall analysis time. To optimize the chromatographic performance and separation properties, analyses were conducted on a Thermo Acclaim™ 120C18 column (150 × 4.6 mm, 5 μm particle size; Thermo Fisher Scientific, USA). The mobile liquid system consisted of 0.1% aqueous formic acid and methanol in a volumetric ratio of 10 : 90 (v/v) delivered under isocratic settings at a flow rate of 0.5 mL min^{-1}, with detection and quantitation of 8-OHdG at a wavelength of 250 nm. A 10 μL injection volume was applied for standard and sample solutions. Under these optimized conditions, the 8-OHdG and pentoxifylline (used as an internal chromatographic standard) compounds were eluted at 3.243 and 3.607 minutes, respectively, and the total run time was within 4 minutes, as illustrated in Fig. S5. In addition, to evaluate the performance of the current HPLC system for the quantification of 8-OHdG in the presence of pentoxifylline as an internal chromatographic standard, several system suitability testing parameters were measured, including resolution (R_s), selectivity factor (α), tailing factor (T), capacity factor (K'), column efficiency (N), and HETP (theoretical plate height). The values for R_s, α, T, K', N, and HETP were 4.36, 1.11, 1, 1.02 to 1.05, 1.70 to 2.01, 18 900 to 19 800, and 0.0079 to 0.0076, respectively; as depicted in Table S1. These values fall within the recommended range,[33] indicating the suitability and effectiveness of the current RP-HPLC method for the identification of the target analyte and internal standard.

3.4 Validation of the new 8-OHdG spectrofluorometric and HPLC testing methods

3.4.1 Evaluation of linear range and detection sensitivity. A stepwise titration of the Ir-SB fluorophore (0.2 μg mL^{-1} in acetate buffer pH 3.6) with 8-OHdG is illustrated in Fig. 2. Upon addition of 8-OHdG from 0.025 to 60 μg mL^{-1}, the intense emission band of the Ir-SB complex (λ_{em} 500 nm) is progressively and monotonically decreased with invariance in the spectral shape, indicating that 8-OHdG does not generate an alternative emissive species. The calibration curve in which $\Delta F = (F_0 - F)$ is plotted against 8-OHdG concentration indicates a sharp rise in the response of the Ir-SB probe at sub-μg mL^{-1} levels of 8-OHdG, then gradually approaches a plateau as the quencher concentration increases, generating a saturation-type

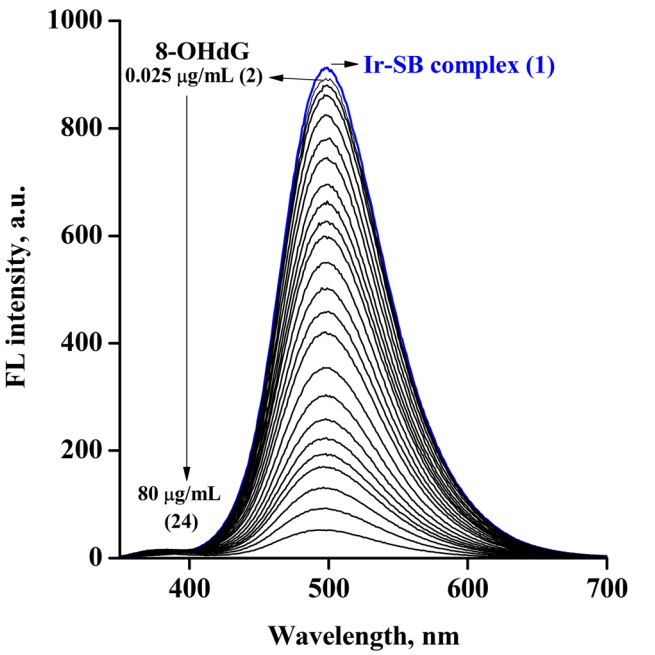

Fig. 2 Fluorescence spectra of 0.2 μg mL^{-1} of Ir-SB complex in the absence and in the presence of different concentrations of 8-OHdG: (1) Ir-SB complex only; (2) 0.025; (3) 0.05; (4) 0.1; (5) 0.4; (6) 1.2; (7) 2; (8) 3; (9) 4; (10) 5; (11) 6; (12) 7; (13) 8; (14) 10; (15) 12; (16) 14; (17) 16; (18) 20; (19) 24; (20) 28; (21) 32; (22) 36; (23) 44; and (24) 60 μg mL^{-1}.

Table 1 Results of assay validation parameters of the proposed spectrofluorometric and HPLC-DAD methods for the determination of 8-OHdG[a]

Parameter	Spectrofluorometric method	HPLC-DAD
Range	0.025–20 μg mL^{-1}	0.005–50 μg mL^{-1}
Slope	31.919	0.846
Intercept	49.814	0.021
r^2	0.9960	0.9997
Recovery %	97.142–100.006	95.321–99.399
RSD%	0.266–2.05	0.604–1.984
LOD*	0.0179 μg mL^{-1}	0.0013 μg mL^{-1}
LOQ*	0.0597 μg mL^{-1}	0.0043 μg mL^{-1}

[a] Accuracy and precision ($n = 3$) were calculated from three different concentration levels, each measured in triplicate within one day and over three successive days.

profile. Importantly, linear regression over the 0.025–20 μg mL^{-1} range showed that the relationship between ΔF and [8-OHdG] is strictly proportional. The best-fit equation ($\Delta F = 31.919C + 49.814$) exhibits exceptional linearity (r^2 of 0.9960) as depicted in Table 1. In the HPLC method, a linear relationship was established between peak areas and 8-OHdG concentrations (using pentoxifylline as the IS, Fig. S6) across the calibration range of 0.005–50 μg mL^{-1}. Besides, the regression equation for the HPLC approach was ($A = 0.846C + 0.021$), and the correlation coefficient ($r^2 = 0.9997$) confirms the strong linear relationship (Table 1). The limits of detection and quantification for 8-OHdG using the spectrofluorometric procedure were 0.0179 and 0.0597 μg mL^{-1}, respectively. In the HPLC procedure, the limit of detection and limit of quantification were determined to be 0.0013 and 0.0043 μg mL^{-1}, respectively. These values confirm the high sensitivity of the two approaches for 8-OHdG quantification.

3.4.2 Accuracy. The accuracies of the developed HPLC-DAD and spectrofluorometric approaches for 8-OHdG were evaluated by calculating the recovery percentage at three different concentrations of 8-OHdG standard, following the calculation procedures outlined in section 2.5. Table 1 summarizes the evaluated recovery percentage results for analyzing 8-OHdG using both spectrofluorometric and HPLC-DAD methods, bearing in mind both intra-day and inter-day variations, indicating excellent accuracy for the two methods with recoveries ranging from 97.142% to 100.006% for spectrofluorometric and 95.321% to 99.399% for HPLC-DAD.

3.4.3 Precision. The precisions of the developed HPLC-DAD and spectrofluorometric approaches were assessed by the relative standard deviation (RSD) for repeatability (intra-day) and intermediate precision (inter-day) following the equation described in section 2.5. Precision was evaluated at three different concentration levels of pure 8-OHdG as presented in Table 1. The precision of both methods was expressed as %RSD. The intra-day and inter-day precision standards for the spectrofluorometric method ranged from 0.266% to 2.05%, while HPLC-DAD showed a slightly wider range of 0.604% to 1.984%. These results together confirm that both established methods exhibit excellent precision in the reliable quantification of 8-OHdG.

3.5 Selectivity and extraction method

The selectivity and analytical validity of the Ir-SB photoprobe toward 8-OHdG were systematically evaluated by examining the effect of various potentially interfering biomolecules on the Ir-SB complex luminescence response. Common biomolecules, including glucose, glycine, histidine, phenylalanine, tyrosine, ascorbic acid, urea, creatinine, and uric acid, were introduced individually into the system containing the Ir-SB complex and Ir-SB complex-8-OHdG under optimized conditions (Fig. S7A and S7B) at a concentration of 40 μg mL^{-1}, except for uric acid which was tested at 5 μg mL^{-1}, corresponding to its tolerance limit. The normalized fluorescence ratio F/F_0 was then calcuated, where F_0 is the intensity of the relevant system and F is the fluorescence intensity recorded after addition of the potential interferent. The consistent luminescence of the Ir-SB complex spectra was subsequently measured. As illustrated in Fig. S7C, for all tested biomolecule species, the black bars corresponding to the Ir-SB complex in the presence of individual biomolecules remained close to unity except in the presence of uric acid, indicating that these biomolecule species alone do not significantly alter the fluorescence of the Ir-SB complex. When each interferent is introduced into the Ir-SB complex-8-OHdG system, the grey bars remain near the 8-OHdG system, except with uric acid, demonstrating that the characteristic quenching produced by 8-OHdG is essentially preserved and that coexisting biomolecule species do not appreciably alter the probe response towards 8-OHdG. A significant quenching in the fluorescence of the Ir-SB complex and the Ir-SB complex-8-OHdG system is observed in the presence of uric acid only. Uric acid and creatinine were found to interfere with 8-OHdG retention time in the HPLC chromatogram due to similar chemical properties or structures, as shown in Fig. S8. So, an effective treatment of urine and serum samples to remove present biomolecules that interfere with 8-OHdG is an essential before 8-OHdG analysis using spectrofluorometric and HPLC-DAD methods. Solid-phase extraction (SPE) was selected as a suitable cleanup strategy due to its operational simplicity, reduced solvent consumption, rapid processing, enhanced selectivity, and compatibility with subsequent analytical procedures. Therefore, several SPE cartridges were evaluated to attain the most efficient system for interference elimination from samples, which has a great quenching effect on Ir-SB complex fluorescence and interferes with 8-OHdG retention time in HPLC chromatograms, including Supelclean™ LC-Florisil (1 g), Supelclean™ ENVI™-18 (500 mg) (Supelco, Bellefonte, PA, USA), and Strata C18-E (500 mg) (Phenomenex, Torrance, USA). Afterwards, acetonitrile, methanol, and isopropanol were separately examined as eluents for each cartridge for separating the 8-OHdG. Based on these trials, 8-OHdG was efficiently extracted with acceptable recovery and negligible interference using the Strata C18-E SPE cartridge with methanol as the eluent, as illustrated in Fig. S9.

3.6 Application of 8-OHdG assay in healthy and diabetic patient biological fluids

To confirm the practical utility of the developed methods, C18-E solid-phase extraction (SPE) was combined with spectrofluorometric and HPLC-DAD analyses to determine 8-OHdG in twenty urine samples and twenty serum samples collected from healthy volunteers and diabetic patients. The obtained data of 8-OHdG quantification in forty biological samples have been illustrated in Table 2. Using the spectrofluorometric method, 8-OHdG was not detected in any serum sample from healthy volunteers, while in diabetic patients, it was detected in five samples, varying between 0.056 and 0.072 μg mL^{-1}. On the other hand, using the developed HPLC-DAD method, 8-OHdG was detected in seven serum samples from healthy volunteers with concentrations ranging from 0.033 to 0.043 μg mL^{-1}, while it was detected in all diabetic patient volunteers falling between 0.037 and 0.065 μg mL^{-1}. In addition, the 8-OHdG amount was detected in most urine samples, whether in healthy or diabetic patients' volunteers, by using spectrofluorimetric and HPLC-DAD methods as depicted in Table 2. Fig. 3 and 4 show representative sections of the full chromatograms presented in Fig. S10 and S11, respectively, confirming the efficiency and reliability of the developed HPLC-DAD technique chromatograms for detecting 8-OHdG in both urine and serum samples of healthy and diabetic patient volunteers. As it is shown in Table 2, urinary sample concentrations of 8-OHdG were consistently higher than those measured in serum samples. Owing to this elevation of the urinary levels, the present Ir-SB complex is a successful optical probe for 8-OHdG quantification in urine samples, and also it has a high degree of selectivity towards 8-OHdG. Finally, the present Ir-SB complex sensor with a urine sample is a successful procedure with simplicity and rapidity, and no special precautions are needed for 8-OHdG demonstration. Moreover, the increased urinary excretion of 8-OHdG may serve as a biological indicator of oxidative stress-induced damage to cellular biomolecules, which associated with the presence of free radicals. Furthermore, the spike recovery experimental trials were conducted to evaluate the accuracy and performance of the extraction cartridge. The percent recovery of 8-OHdG ranged between 92.13% and 97.89%, while relative standard deviation (RSD) values were within 0.93–2.78%, reflecting satisfactory precision and extraction efficiency. Collectively, these results demonstrate that the proposed spectrofluorometric and HPLC-DAD methods, using the optimized SPE cartridge, provide reliable and suitable analytical techniques for the quantification of 8-OHdG in biological fluids.

In addition, statistical analysis and comparison between healthy and diabetic groups as well comparison between fluorescence and HPLC method were achieved (see SI file) and the main finding was as follows: (1) diabetes is associated with significantly elevated oxidative DNA damage measurable by 8-OHdG in both serum (1.8×) and urine (32×). (2) ROC-optimized cutoffs provide superior diagnostic performance compared to conventional approaches; Serum HPLC-DAD at 0.0420 μg mL^{-1} achieves 90% sensitivity and 70% specificity (AUC = 0.890), representing the optimal balance for clinical screening. (3) HPLC-DAD is the superior analytical method due to superior sensitivity and discrimination; Serum HPLC-DAD Youden's index (0.600) exceeds all other methods. (4) Urine methods

Table 2 Determination of 8-OHdG in serum and urine of human healthy and diabetic patient volunteers by the proposed spectrofluorometric and HPLC-DAD methods[a]

		Healthy volunteers (μg mL^{-1})		Patient volunteers (μg mL^{-1})	
Sample type[a]	Sample no.	FL	HPLC-DAD	FL	HPLC-DAD
Serum	1	nd	0.041 ± 0.001	nd	0.042 ± 0.0009
	2	nd	0.037 ± 0.0002	nd	0.045 ± 0.001
	3	nd	0.043 ± 0.0003	0.061 ± 0.002	0.058 ± 0.0001
	4	nd	nd	0.056 ± 0.001	0.051 ± 0.0002
	5	nd	0.045 ± 0.0002	0.058 ± 0.0001	0.055 ± 0.0001
	6	nd	0.033 ± 0.0006	0.061 ± 0.005	0.063 ± 0.0007
	7	nd	nd	0.071 ± 0.003	0.065 ± 0.001
	8	nd	0.038 ± 0.0006	nd	0.047 ± 0.0001
	9	nd	nd	nd	0.042 ± 0.0003
	10	nd	0.042 ± 0.0006	nd	0.037 ± 0.0007
Urine	1	0.201 ± 0.003	0.180 ± 0.002	7.183 ± 0.153	6.583 ± 0.133
	2	0.057 ± 0.002	0.056 ± 0.005	15.921 ± 0.115	15.766 ± 0.106
	3	nd	0.034 ± 0.005	0.402 ± 0.001	0.372 ± 0.001
	4	nd	0.017 ± 0.001	0.160 ± 0.003	0.154 ± 0.003
	5	0.112 ± 0.001	0.105 ± 0.001	1.925 ± 0.017	2.025 ± 0.028
	6	0.151 ± 0.001	0.175 ± 0.003	0.265 ± 0.003	0.244 ± 0.004
	7	nd	nd	12.091 ± 0.055	12.655 ± 0.067
	8	0.262 ± 0.003	0.284 ± 0.004	0.076 ± 0.004	0.071 ± 0.003
	9	0.352 ± 0.006	0.332 ± 0.008	0.134 ± 0.001	0.128 ± 0.001
	10	nd	0.013 ± 0.001	0.063 ± 0.001	0.069 ± 0.001

[a] 'nd' means 'not detected'.

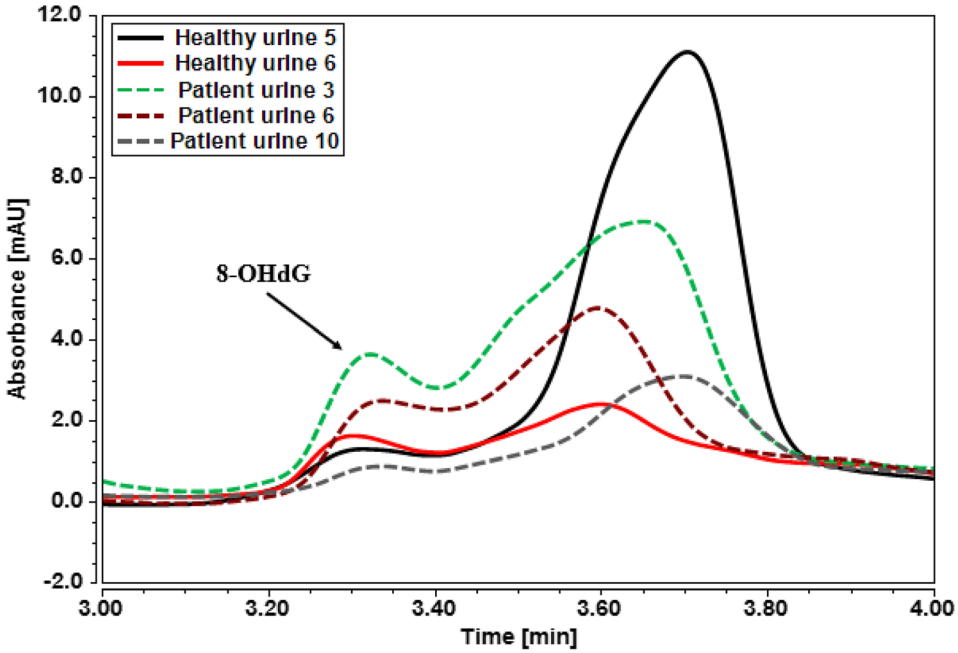

Fig. 3 HPLC chromatogram of 8-OHdG in urine samples of healthy and diabetic patient's volunteers.

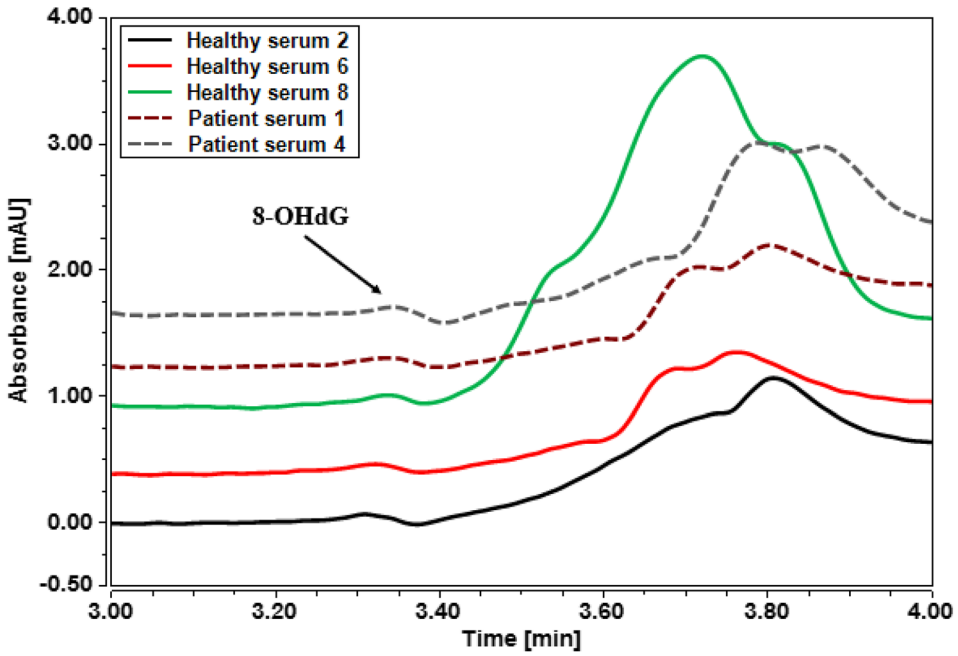

Fig. 4 HPLC chromatogram of 8-OHdG in serum samples of healthy and diabetic patient volunteers.

serve as excellent confirmatory tests with perfect specificity (100%) and PPV (100%) at cutoffs of 0.3720–0.4020 μg mL^{-1}, ideal for ruling in diabetes when serum results are equivocal. (5) The two analytical methods correlate excellently ($r > 0.90$), but the choice of cutoff significantly impacts clinical utility; ROC-derived thresholds are essential for effective biomarker implementation. On other hand, clinical implementation calculation showed that serum HPLC-DAD at 0.0420 μg mL^{-1} should be used for primary diabetes screening (90% detection rate), with urine HPLC-DAD at 0.3720 μg mL^{-1} reserved for confirmatory testing (100% specificity).

3.7 Comprehensive study of fluorescence quenching mechanism

The Stern–Volmer plots presented in Fig. S12, together with the corresponding data listed in Table 3, offer clear mechanistic clarification regarding the fluorescence quenching behavior[34,35] of the Ir-SB complex by 8-OHdG. At all four temperatures (296,

Table 3 Stern–Volmer quenching constants for the interaction of 8-OHdG with Ir-SB complex at different temperatures

T (K)	$K_{SV} \times 10^4$ L mol^{-1}	r^2
296	1.575	0.998
303	1.543	0.997
308	1.539	0.997
313	1.425	0.995

303, 308, and 313 K), the ratio F_0/F increases linearly with the 8-OHdG concentration over the range 0.141–2.82 $\times$ 10^{-5} M, and the correlation coefficients ($R \approx$ 0.995–0.998) demonstrate that the classical Stern–Volmer expression $F_0/F = 1 + K_{SV}$ [8-OHdG] adequately describes the system under the chosen conditions. According to the Stern–Volmer mechanism, quenching systems are classified as either dynamic (diffusion) or static (ground state complex), depending on the temperature effect of quenching behavior. In static quenching, increasing temperature typically reduces complex stability, resulting in lower values of quenching constant (K_{SV}). Conversely, in dynamic quenching, elevated temperatures increase the quenching constant values (K_{SV}) due to enhanced molecular diffusion. The experimental findings revealed that the K_{SV} decreased from 1.575 $\times$ 10^4 to 1.425 $\times$ 10^4 L mol^{-1} as the temperature increased from 296 to 313 K, indicating that the fluorescence quenching of the Ir-SB complex by 8-OHdG proceeds predominantly through a static mechanism involving formation of a non-emissive ground-state Ir-SB/8-OHdG association complex. Because no distinct new absorption band was observed upon addition of 8-OHdG, the term "ground-state complex" is used cautiously here to describe a weak, non-emissive, non-covalent ground-state association/contact interaction rather than the formation of a new spectroscopically distinguishable chemical species.

However, for the static quenching interaction, if it is assumed that there are similar and independent binding sites in the Ir-SB complex, the binding constant (K_a) and the number of binding sites (n) could be determined according to the following equation:[36] $\log((F_0 - F)/F) = \log K_a + n \log$[8-OHdG], where in the present case, K_a and n are the binding constant and the number of binding sites, respectively. A plot of $\log((F_0 - F)/F)$ *versus* log[8-OHdG] (Fig. S13) gives a straight line, whose slope equals n and the intercept on the Y-axis equals $\log K_a$, and the calculated values are itemized in Table S2. The calculated binding constants showed a clear increasing trend with rising temperature. This progressive increase indicates that higher temperatures favor the interaction between the Ir-SB complex and 8-OHdG and enhance the binding affinity of the system. The calculated n values approach unity at elevated temperature, suggesting an approximately 1 : 1 binding interaction between Ir-SB complex and 8-OHdG. The deviation of n from exactly 1 may be attributed to the apparent nature of the binding parameter and possible non-ideal behavior of the system under the studied conditions.

Importantly, the temperature dependence of K_a should not be interpreted as contradicting the static-quenching assignment. K_{SV} and K_a are not strictly identical physical parameters in a real fluorescence sensing system. K_{SV} reflects the efficiency of fluorescence quenching, whereas K_a reflects the apparent association affinity between Ir-SB and 8-OHdG. Therefore, an increase in apparent binding affinity with temperature can occur while the fluorescence-quenching efficiency of the associated complex decreases slightly. In this system, the decrease in K_{SV} with temperature remains the principal evidence for assigning static quenching as the predominant pathway, while the binding data confirm the existence of Ir-SB/8-OHdG association.

The thermodynamic parameters further support the occurrence of spontaneous non-covalent association between Ir-SB and 8-OHdG. From the van't Hoff plot of $\ln K_a$ *versus* $1/T$, the positive values of $\Delta H°$ and $\Delta S°$ were calculated as +138.13 kJ mol^{-1} and +511.18 J mol^{-1} K^{-1}, respectively (Table S2). The positive $\Delta H°$ indicates that the association process is endothermic, while the positive $\Delta S°$ suggests that the interaction is mainly entropy-driven, most likely due to desolvation and release of ordered solvent molecules from the interacting surfaces during Ir-SB/8-OHdG association. In addition, the negative $\Delta G°$ values, ranging from −13.61 to −22.19 kJ mol^{-1} over the investigated temperature range, confirm that the binding process is spontaneous. These thermodynamic features are consistent with weak non-covalent association involving hydrogen bonding, π-related interactions, van der Waals contacts, and solvent reorganization/desolvation effects,[37] rather than formation of a new strongly bound or spectroscopically distinguishable complex. Since both Ir-SB and 8-OHdG are expected to be predominantly neutral under the optimized experimental conditions, direct charge–charge electrostatic attraction is not invoked as the dominant binding force.

The inner filter effect was also evaluated because 8-OHdG absorbs in the excitation region of the Ir-SB probe. The fluorescence attenuation may therefore include a partial primary inner filter contribution, in which the analyte absorbs part of the incident excitation light before it reaches the fluorophore. However, IFE is not considered the dominant mechanism, because the temperature-dependent Stern–Volmer data support static quenching, and the selectivity study shows that the response is not governed merely by nonspecific spectral overlap.

Fig. S14 presents Stern–Volmer plot for the apparent fluorescence decrease together with Lakowicz correction parameter used to account for optical attenuation, indicating that the observed signal loss should be examined in terms of absorption-based distortion as well as apparent quenching. Lakowicz correction can be calculated from the following formula:

$F_{corr} = F_{obs} \times 10^{(A_{ex}+A_{em})/2}$, where F_{obs} is the measured fluorescence intensity, F_{corr} is the corrected fluorescence intensity, and A_{ex} and A_{em} are the absorbances at the excitation and emission wavelengths, respectively. All calculations are presented in Table S3.

Fig. S14 shows that the absorption spectrum of 8-OHdG has a maximum at the same wavelength used for excitation of the Ir-SB probe, while the excitation spectrum of the probe is recorded under the corresponding emission conditions. This means

there is a direct overlap between the absorbance band of 8-OHdG and the excitation band of the probe, so 8-OHdG can effectively compete for the excitation light. Under these conditions, part of the fluorescence decrease can arise from a primary inner filter effect because 8-OHdG partially screens the excitation beam before it reaches the fluorophore.

Accordingly, the observed fluorescence attenuation of the Ir-SB complex by 8-OHdG is best interpreted as a predominantly static quenching process with a secondary contribution from the primary inner filter effect. The decrease in K_{SV} with increasing temperature indicates that quenching is mainly governed by weak ground-state association/contact interaction, as expected for a static process. However, because 8-OHdG exhibits substantial absorption at the excitation wavelength of the probe, part of the apparent signal decrease also originates from absorption-induced attenuation. Thus, the fluorescence response reflects both molecular association between Ir-SB and 8-OHdG and partial optical attenuation, but the dominant quenching pathway is assigned to static weak ground-state association/contact interaction rather than formation of a new spectroscopically distinguishable complex.

3.8 Comparison with previously published methods

Table 4 presents a comparative evaluation of the developed methods against previously reported techniques for 8-OHdG quantification. Briefly, the response time between the developed sensor and 8-OHdG was 30 s which is shorter than those reported for 38 nt and 66 nt aptamers,[24] cysteamine stabilized gold nanoparticles,[25] Apt-K^+-NMM system,[26] carbon dots and amine functionalized gold nanoparticles[27] which require more than 10 min for binding. Also, the preparation of the Ir-SB complex sensor in our method is simple and time-saving when compared with reported methods.[20,21] Additionally, our sensor provides a wide linear range (0.025–20 μg mL^{-1}) when compared with electrochemical method[22] and fluorometric method.[27] Therefore, the two new approaches excel not only in their time efficiency, operational simplicity, and minimal safety precautions but also in their adequate sensitivity, high selectivity, broad linear range, and versatility across diverse sample matrices—rendering them practical and reliable for routine 8-OHdG analysis.

3.9 Environmental sustainability evaluation of the proposed approaches

Multiple green assessment metrics were used for examining the environmental profile of the proposed analytical procedures, as illustrated in Fig. 5A, the method achieved an overall AGREE[38] score of 0.62, reflecting a satisfactory level of compliance with green analytical chemistry principles in the quantitation of 8-OHdG. Notably, only one criterion (NO. 3) was categorized as red, arising from the off-line quantitative workflow. Additionally, two yellow subsections, criteria 1 and 10, were documented due to the offline sampling strategy and only some reagents are environmentally bio-based. Overall, the AGREE output confirms that the green footprint of the developed approach remains within acceptable sustainability limits.

The analytical green star area (AGSA)[39] score was 63.89 (Fig. 5B), indicating the environmentally acceptable nature of established methodology.

In addition, the Multi-Color Assessment platform (MA) was applied for the assessment of not only greenness but also practicality, analytical performance, and innovation.[40] As illustrated in Fig. 5C the MA platform represented the whiteness assessment score of the methods developed to determine 8-OHdG. According to results displayed in Fig. 5C, the method demonstrated outstanding environmental performance according to the GEMAM index, attaining a score of 80.7%. Later, the advanced technique's BAGI score reached 67.5%, confirming the method's operational feasibility and suitability for practical implementation. Moreover, the established technique's RAPI value was 77.5%, demonstrating robust analytical validation and performance characteristics. Moreover, the VIGI

Table 4 Comparison between developed methods and reported previous methods

Techniques	Linear range, μg mL^{-1}	LOD, μg mL^{-1}	Sample	Ref.
Capillary electrophoresis with UV detection	10–500	5	Urine	14
Capillary electrophoresis	0.1–50.0	0.19	Urine	15
HPLC-ECD	0.002–0.2	0.0001	Urine	16
HPLC-PDA	0.1–5	0.04	Urine	17
HPLC-DAD	0.0028–0.25	0.00085	Urine	18
LC-MS/MS	0.01–0.25	0.01	Saliva and urine	19
Electrochemical	0.001–14.16	0.0002	Urine and serum	20
Electrochemical	0.014–152	0.01	Urine	21
Electrochemical	0.05–1	0.014	Serum	22
Electrochemical	0.085–28.32	0.0255	Saliva	23
Colorimetry	0.0042–0.028	0.0037	Urine	24
Colorimetry	0.0042–0.028	0.0029	Urine	25
Fluorometry	0.001–0.06	0.00034	Urine	
Fluorometry	0.03–0.57	0.0045	Urine	27
HPLC-DAD	0.005–50	0.0013	Biofluids from healthy and diabetic patient volunteers	Current work
Spectrofluorometry	0.025–20	0.0179		

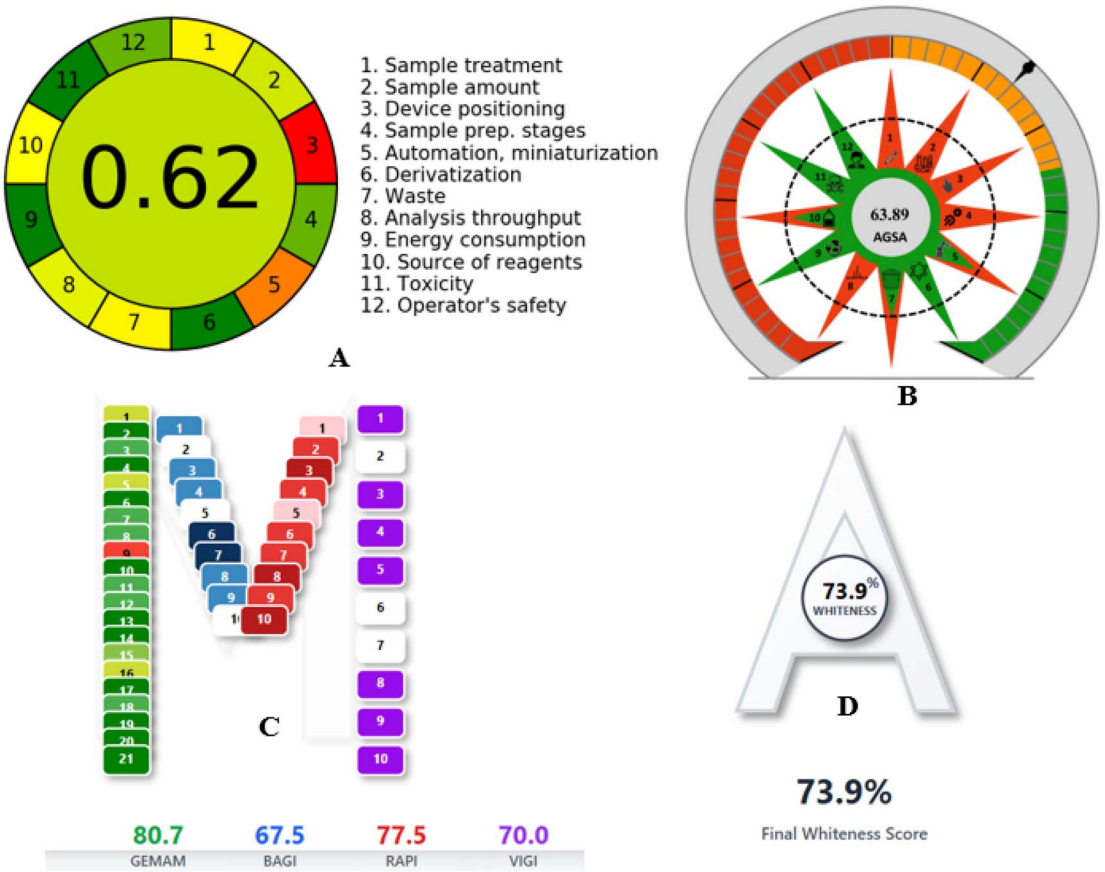

Fig. 5 Greenness scores and MA whiteness assessment score of the method developed to determine 8-OHdG. (A) AGREE pictogram; (B) analytical green star area (AGSA); (C) Multi-Color Assessment platform (MA); and (D) overall MA whiteness score.

score of 70% indicated a good degree of technological advancement and innovation. The overall MA Whiteness Score calculated as the arithmetic mean of all four indices for this method was established to be 73.9% (Fig. 5D), signifying a well-balanced analytical platform that integrates sustainability, functionality, reliability, and innovation.

4 Conclusion

In conclusion, the developed spectrofluorimetric and HPLC-DAD approaches coupled with the Strata C18-E SPE cartridge demonstrate excellent analytical characteristics, including wide linear dynamic ranges, high sensitivity, superior selectivity, reliable accuracy, satisfactory stability, and precision. Furthermore, both methods were successfully applied to the quantitation of 8-OHdG in biofluids collected from healthy individuals and diabetic patients, confirming their practical applicability in real biological matrices. The two developed strategies comply with the principles of green and white analytical chemistry by decreasing environmental impact while increasing analytical efficiency and safety.

These findings establish the proposed methods as reliable, sustainable, and practically applicable tools suitable for routine monitoring and bioanalytical determination of 8-OHdG.

Conflicts of interest

There are no conflicts to declare.

Data availability

Data supporting the findings of this study are available upon request.

Supplementary information (SI) is available. See DOI: https://doi.org/10.1039/d6ra02144a.

Acknowledgements

This article is derived from a research grant funded by the Research, Development, and Innovation Authority (RDIA)—Kingdom of Saudi Arabia—with grant number (13395-MED-2023-JFU-R-3-1-HW) and funded by the Deanship of Graduate Studies and Scientific Research at Jouf University under grant No. (DGSSR-2025-FC-01019). The authors would also like to acknowledge the support and facilities provided by the Central Laboratory at Jouf University.

References

1 S.-H. Park, J.-H. Kim, G. Y. Chi, G.-Y. Kim, Y.-C. Chang, S.-K. Moon, S.-W. Nam, W.-J. Kim, Y. H. Yoo and Y. H. Choi, *Toxicol. Lett.*, 2012, **212**, 252–261.
2 M. A. Hayat, *Autophagy: Cancer, Other Pathologies, Inflammation, Immunity, Infection, and Aging*, Academic Press, 2017, vol. 12.
3 M. Gutowski and S. Kowalczyk, *Acta Biochim. Pol.*, 2013, **60**, 1–16.
4 M. Valko, C. J. B. Rhodes, J. Moncol, M. M. Izakovic and M. Mazur, *Chem. Biol. Interact.*, 2006, **160**, 1–40.
5 O. Zitka, S. Krizkova, S. Skalickova, P. Kopel, P. Babula, V. Adam and R. Kizek, *Comb. Chem. High Throughput Screen.*, 2013, **16**, 130–141.
6 P. M. W. Lam, V. Mistry, T. H. Marczylo, J. C. Konje, M. D. Evans and M. S. Cooke, *Free Radic. Biol. Med.*, 2012, **52**, 2057–2063.
7 J. E. Klaunig and L. M. Kamendulis, *Annu. Rev. Pharmacol. Toxicol.*, 2004, **44**, 239–267.
8 K. Roszkowski, W. Jozwicki, P. Blaszczyk, A. Mucha-Malecka and A. Siomek, *Med. Sci. Monit.*, 2011, **17**, CR329.
9 M. D. Evans and M. S. Cooke, *Bioessays*, 2004, **26**, 533–542.
10 J. Xu, J. Zhang, R. Zeng, L. Li, M. Li and D. Tang, *Sens. Actuators, B Chem.*, 2022, **368**, 132141.
11 S. Mei, Q. Yao, C. Wu and G. Xu, *J. Chromatogr. B*, 2005, **827**, 83–87.
12 C.-J. Wang, N.-H. Yang, C.-C. Chang, S.-H. Liou and H.-L. Lee, *J. Chromatogr. B*, 2011, **879**, 3538–3543.
13 Q.-H. Yao, S.-R. Mei, Q.-F. Weng, P. Zhang, Q. Yang, C. Wu and G.-W. Xu, *Talanta*, 2004, **63**, 617–623.
14 V. Kvasnicová, E. Samcová, A. Jursová and I. Jelínek, *J. Chromatogr., A*, 2003, **985**, 513–517.
15 M.-J. Li, J.-B. Zhang, W.-L. Li, Q.-C. Chu and J.-N. Ye, *J. Chromatogr., B*, 2011, **879**, 3818–3822.
16 O. Zengi, A. Karakas, U. Ergun, M. Senes, L. Inan and D. Yucel, *Clin. Chem. Lab. Med.*, 2011, **50**, 529–534.
17 B. Mendes, P. Silva, I. Mendonça, J. Pereira and J. S. Câmara, *Talanta*, 2013, **116**, 164–172.
18 N. N. Al-Hashimi, R. O. Shahin, A. H. El-Sheikh, M. J. Jibreel, N. A. Alsakhen, A. M. Alqudah, M. K. Oqal and J. I. Abdelghani, *Acta Chromatogr.*, 2024, **36**, 218–227.
19 K. Kahremanoglu, E. R. Temel, T. E. Korkut, A. A. Nalbant, B. B. Azer, C. Durucan, M. Volkan and E. Boyaci, *J. Sep. Sci.*, 2020, **43**, 1925–1933.
20 N. Nontawong, M. Amatatongchai, P. Jarujamrus, D. Nacapricha and P. A. Lieberzeit, *Sens. Actuators, B Chem.*, 2021, **334**, 129636.
21 R.-N. Zhao, L.-P. Jia, Z. Feng, R.-N. Ma, W. Zhang, L. Shang, Q.-W. Xue and H.-S. Wang, *Biosens. Bioelectron.*, 2019, **144**, 111669.
22 G. V Martins, A. P. M. Tavares, E. Fortunato and M. G. F. Sales, *Sci. Rep.*, 2017, **7**, 14558.
23 C. Varodi, F. Pogacean, M. Coros, M.-C. Rosu, R.-I. Stefan-van Staden, E. Gal, L.-B. Tudoran, S. Pruneanu and S. Mirel, *Sensors*, 2019, **19**, 4297.
24 P. Matulakul, D. Vongpramate, S. Kulchat, A. Chompoosor, R. Thanan, P. Sithithaworn, C. Sakonsinsiri and T. Puangmali, *ACS Omega*, 2020, **5**, 17423–17430.
25 C. Sakonsinsiri, T. Puangmali, K. Sreejivungsa, S. Koowattanasuchat, R. Thanan, A. Chompoosor, S. Kulchat and P. Sithithaworn, *RSC Adv.*, 2022, **12**, 25478–25486.
26 H. Liu, Y.-S. Wang, X. Tang, H.-X. Yang, S.-H. Chen, H. Zhao, S.-D. Liu, Y.-F. Zhu, X.-F. Wang and Y.-Q. Huang, *J. Pharm. Biomed. Anal.*, 2016, **118**, 177–182.
27 S. Ngernpimai, J. Thonghlueng, Y. Phothikul, A. Chompoosor, R. Thanan, T. Puangmali and C. Sakonsinsiri, *ACS Appl. Nano Mater.*, 2023, **6**, 7055–7064.
28 A. Hamza, A. A. Al-Sibaai, H. Alwael, Z. M. Saigl, E. H. Alosaimi, M. S. Refat and M. S. El-Shahawi, *Results Chem.*, 2022, **4**, 100422.
29 B. Musikavanhu, Y. Liang, Z. Xue, L. Feng and L. Zhao, *Molecules*, 2023, **28**, 6960.
30 M. Xu, J.-T. Liao, G. Chen, Y.-Y. Chen, D. Liu and L.-L. Wang, *Front. Chem.*, 2022, **10**, 867808.
31 G. M. Khairy, A. S. Amin, S. M. N. Moalla, A. Medhat and N. Hassan, *RSC Adv.*, 2022, **12**, 27679–27686.
32 D. Das, A. K. Sharma, K. K. Chattopadhyay and D. Banerjee, *J. Alloys Compd.*, 2023, **960**, 170689.
33 C. K. Sahoo, M. Sudhakar, D. V. Ramana, K. Satyanarayana and K. C. Panda, *Asian J. Pharm. Anal. Med. Chem.*, 2018, **8**, 109–116.
34 Y.-Q. Wang, H.-M. Zhang, G.-C. Zhang, W.-H. Tao, Z.-H. Fei and Z.-T. Liu, *J. Pharm. Biomed. Anal.*, 2007, **43**, 1869–1875.
35 D. Shcharbin, B. Klajnert, V. Mazhul and M. Bryszewska, *J. Fluoresc.*, 2005, **15**, 21–28.
36 H. Du, J. Xiang, Y. Zhang and Y. Tang, *Bioorg. Med. Chem. Lett.*, 2007, **17**, 1701–1704.
37 R. Claveria-Gimeno, S. Vega, O. Abian and A. Velazquez-Campoy, *Expert Opin. Drug Discov.*, 2017, **12**, 363–377.
38 F. Pena-Pereira, W. Wojnowski and M. Tobiszewski, *Anal. Chem.*, 2020, **92**, 10076–10082.
39 F. R. Mansour, A. Bedair, F. Belal, G. Magdy and M. Locatelli, *Sustain. Chem. Pharm.*, 2025, **46**, 102051.
40 A. E. F. Abbas, G. Magdy and M. K. Halim, *Microchem. J.*, 2025, 114781.